Segmentation of Astrocyte Cells in Fluorescently Labeled Images

Muhammed Pesen
Computer Engineering
Istanbul Medipol University
Istanbul/Turkey
muhammed.pesen@std.medipol.edu.tr

Cihan Bilge Kayasandık
Computer Engineering
Istanbul Medipol University
Istanbul/Turkey
cbkayasandik@medipol.edu.tr

2024 Medical Technologies Congress (TIPTEKNO) | 979-8-3315-2981-9/24/$31.00 ©2024 IEEE | DOI: 10.1109/TIPTEKNO63488.2024.10755324

***Abstract*—Astrocytes, the most abundant brain cells, play crucial roles beyond mere support for neurons. Despite their significance, understanding them remains challenging due to imaging and analysis limitations. In this study, we developed a segmentation model that improves upon existing methods and conducted a comprehensive comparison of approaches from the literature, predominantly focusing on various U-net architecture variants. By optimizing configurations, loss functions, and processing steps, our U-net with Inception layers achieved an 83% F1 score, excelling in densely populated regions. The effectiveness of the developed segmentation model was assessed by applying it to images of astrocyte cells with different morphologies taken from serum-containing and serum-free cultures. By applying the Directional Ratio method to the segmented cells, it was determined that astrocytes in serum-free cultures exhibited greater anisotropy, thus demonstrating how serum influences astrocyte morphology through computational methods. Our findings emphasize the importance of multi-scale analysis in cell segmentation. The proposed method effectively segments and analyzes astrocyte images, revealing significant morphological changes influenced by serum, and offers a valuable tool for neuroscience studies by minimizing manual errors and enabling large-scale analysis.**

***Keywords*—Astrocyte segmentation, Deep learning, Morphological Analysis, U-net**

I. Introduction

Astrocytes, the most abundant cells in the human brain, are vital for understanding brain pathways. Once considered passive support for neurons, they are now recognized for crucial roles in neuronal development, function, and synaptic regulation in the Central Nervous System (CNS). Astrocytes modulate neuronal connections through their structural design, which reflects their diverse functions. Morphological changes in astrocytes are linked to CNS trauma, infection, stroke, autoimmune responses, and neurodegenerative diseases, making them prime targets for neurological therapies [1, 2, 3]. Despite their importance, much remains unknown about astrocytes, especially their interactions with neurons, due to immature imaging techniques. Efficient image analysis methods are needed to overcome the limitations of current tools, which waste time and resources by failing to detect complex astrocyte structures.

While neuron cell segmentation methods are well-developed, astrocyte segmentation remains challenging due to their intricate morphology. Traditional thresholding and morphological operations are inadequate for astrocyte detection, even with fluorescent labeling [4, 5, 6]. Studies focusing on astrocyte cell fibrils, like those using threshold-based segmentation, address only cell classification, tolerating inaccurate segmentation [7]. Techniques like the one by Sethi et al. [8], which extract cell skeletons for Sholl analysis, discard crucial morphological information such as extension thickness, which is important for understanding cell cycles in neurological disorders [9]. The cell body, too, exhibits significant morphological properties that cannot be captured from the skeleton alone.

With the rise of artificial neural networks, convolutional neural networks now dominate cell segmentation. Early applications targeted astrocyte detection without segmentation [6]. Kayasandik et al. [10] later introduced a multi-step deep learning model with cascaded U-Nets and Framelet filters. However, that model is only designed to segment star-shaped astrocytes and is not suitable to segment different shaped cells.

In our work, instead of comparing our method with others from the literature, we focused on evaluating the performance of commonly used U-Net variants on our dataset, as all existing methods are based on U-Net. By integrating preprocessing and postprocessing methods, data augmentation, and optimizing network architecture with additional Inception layers and combined loss functions, we developed a novel model that outperforms others in the literature. Including inception layers notably improved segmentation accuracy, especially for adjacent cells in crowded regions. We validated our method by segmenting fluorescently labeled astrocytes, revealing serum-deviation's impact on astrocyte cultures. Our method successfully captured morphological differences caused by serum inclusion during culture preparation.

II. Data Preparation

A. Sample preparation and Imaging

In this study, we used a dataset provided by researchers at REMER (Medipol Regenerative and Restorative Medicine Research Center). Cells from the hippocampus of a newborn

(p0-p3) FVB-Tg(Prism)1989Htz/J transgenic mice were obtained using REMER's standard primary hippocampal culture protocol. Two cultures were prepared for method validation, one of which was serum-free. The transgenic mice expressed DsRedMax and YFP sequences in the Aldh1/1 genes, allowing easy identification of astrocytes through fluorescence. Cells were imaged with a 561nm laser on a Spinning Disk microscope at 40x magnification using an EMCCD camera and tiling.

III. Cell Segmentation

The whole cell segmentation step is formed by preprocessing, segmentation by deep learning model, and postprocessing steps. For a fair comparison of different neural network architectures, identical pre- and post-processing steps were applied throughout the analysis.

A. Preprocessing

The images were smoothed using Gaussian filtering for soft denoising. Due to the dataset's low and uneven contrast distribution, which poses challenges for segmentation, histogram equalization is applied to enhance contrast. This process was done locally to ensure accurate segmentation of low-contrasted regions.

B. Segmentation

For the segmentation task, we used six different artificial neural network architectures, all based on U-Net. U-Net consists of two main components: an encoder path, similar to a Convolutional Neural Network (CNN), and a decoder path. The encoder path includes blocks with two 3x3 convolutions followed by an activation function, like ReLU, doubling the number of channels at each step. A 2x2 max pooling layer with a stride of 2 is applied between blocks. In the decoder path, 3x3 transposed convolutions with a stride of 1 halve the number of channels, followed by the concatenation of cropped skip connections from the encoder and two rounds of 3x3 convolution with ReLU activation [11].

In addition to Vanilla U-Net, we used modified U-Net architectures with weights transferred from VGG16 and VGG19 [12], evaluated dense skip connections using U-Net++ [13], and tested the impact of integrating Inception and ResNet layers into the U-Net encoder [14]. The architectures and their key differences from Vanilla U-Net are summarized in Table I.

To assess the effect of the loss function, we used binary cross-entropy and dice loss, the latter chosen for its focus on overlap accuracy between predicted and actual segments [15]. However, over-segmentation in densely packed cell regions was identified during analysis. To address this, Focal Loss was introduced to improve performance by emphasizing hard-to-classify samples [16]. We also tested a combination of Focal and Dice losses, which enhanced precision in distinguishing adjacent cellular structures.

Our dataset included eight 1024x1024 pixel images, each containing around 200 astrocytes, resulting in 1600 astrocytes for model training. Images were divided into 256x256 pixel patches, with an optimized overlap of 128 pixels, ensuring full inclusion of astrocytes without discontinuity (Fig. 1 (a)-(b)). Data augmentation techniques, including Elastic Transform, Horizontal Flip, Random Brightness Contrast, and Coarse Dropout, were applied, with a focus on Elastic Transform to simulate realistic cellular deformations. This process yielded 2400 training samples, with 20% reserved for validation and parameter optimization, and the remainder used for training the models.

TABLE I: Analyzed Architectures and Key Features

Name	Architecture signature
Vanilla U-Net	4-layer Encoder and Decoder
U-Net-VGG16	VGG16 Encoder with transfer learning
U-Net-VGG19	VGG19 Encoder with transfer learning
U-Net++	Dense skip connections
U-Net-Inceptionv4	Multi-scale kernels
U-Net-Inception-ResNet-v2	Multi-scale kernels, Identity shortcuts

C. PostProcessing

Postprocessing was applied to relocate overlapping patches, classifying pixels as foreground if marked in any segmented patch to reduce false negatives and ensure seamless merging (Fig. 1 (d)). After patch relocation, the binary segmented image was generated. Finally, connected component analysis was applied to remove regions smaller than a numerically optimized threshold, based on the approximate minimum area of an astrocyte cell (Fig. 1 (e)).

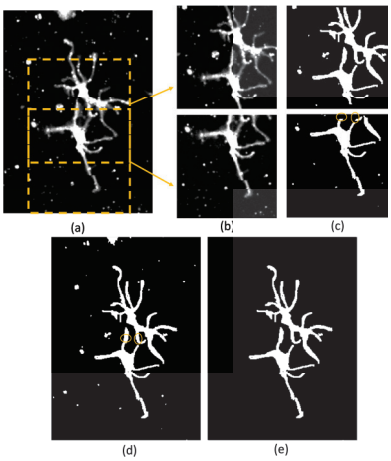

Fig. 1: Postprocessing step: (a) Overlapping patches in a sample image (for simplicity, only two patches are shown). (b) Extracted patches from the raw image. (c) Segmented patches with errors in the cell bodies circled in yellow. (d) Patches are relocated as explained in the Method. As seen the errors in the overlapping regions of one patch is compensated by the subsequent patch. (e) Small regions are eliminated by connected component analysis.

IV. Results

For training all models, we used the Adam optimizer with a learning rate of 0.0001 and a weight decay of 0.0001 for L2 regularization. Various loss functions were tested to determine the most effective one. The batch size was set at 12, and the number of epochs varied based on the convergence of loss and accuracy on the validation set. The connected component analysis threshold was optimized at 500 pixels. The model configuration with the best validation set performance was saved for further use. The project was implemented using Pytorch 2.0.1 and Python 3.11.5, with an NVIDIA Tesla K80 GPU.

Our test dataset consisted of 256 images, containing about 800 astrocytes. U-Net with binary cross-entropy loss was used as the baseline, and all other configurations were compared against it. During analysis, the best performance was achieved when architectures were trained with the average of dice and focal loss functions. Table II shows the performance of each model with this combined loss function.

TABLE II: Model Performances with the Average of Dice and Focal Loss

Model	Performance Metrics		
	Precision	Recall	F1 score
Vanilla U-Net	91%	72%	80%
U-Net-VGG16	92%	72%	81%
U-Net- VGG19	96%	62%	76%
U-Net++	97%	65%	78%
U-Net- Inceptionv4	90%	76%	83%
U-Net Inception-ResNet-v2	93%	73%	81%

To validate the introduced model, we used an experimental dataset of morphologically distinct astrocytes (see Fig. 2 (a)-(b)), with the aim of having the model automatically identify these differences. Fluorescently labeled astrocyte images from transgenic mice were collected from two culture settings: with and without serum. Sixteen images from each setting, captured at 40x magnification and 1024x1024 pixel resolution, matched the training image acquisition conditions. We needed a large image set to analyze isolated astrocytes, excluding clusters, and segmented 100 isolated astrocytes from each group for a balanced dataset.

The best model, a U-Net-Inception architecture trained with a combination of dice and focal losses, was applied to the experimental dataset. Images were preprocessed, segmented, and postprocessed as described in the previous section, with the only modification being an optimization of the connected component analysis threshold to accurately detect individual astrocytes and remove artifacts.

Isolated astrocytes were analyzed for isotropy using the Directional Ratio (DR), a local morphological measure derived from multi-scale directional analysis [17, 18]. This technique involves filtering the image with oriented rectangular filters distributed evenly in space. The DR is defined as the ratio of the minimum to maximum filtering responses, ranging from 0 to 1. A DR of 1 indicates perfect isotropy within the local neighborhood, with equal minimum and maximum responses. A lower DR signifies greater anisotropy. For our analysis, the filter scale was optimized to 30x4 pixels based on average cell body size and branch width, and the analysis was performed across 10 numerically optimized orientations. Pixels with a DR greater than 0.94 were classified as isotropic, while those below this threshold were deemed anisotropic (Fig. 2 (e)-(h)). Each cell was analyzed individually to prevent influence from adjacent cells, and results were averaged within each group.

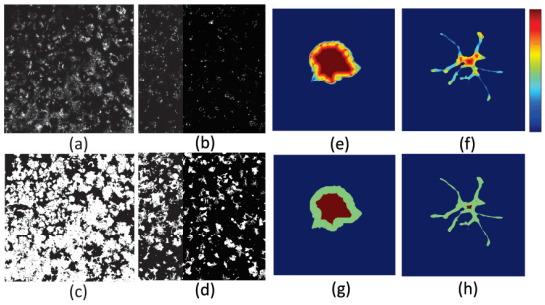

Fig. 2: Segmentation and isotropy analysis of astrocyte cell regions. (a) A raw image acquired from culture with serum, (b) a raw image acquired from a culture without serum, (c)-(d) segmented images of (a)-(b) respectively, (e)-(f) examples of Directional Ratio (DR) analysis of isolated segmented astrocytes from the corresponding images. Red regions show high isotropy while blue shows anisotropy. (g)-(h) The pixels with DR value larger than 0.94 are determined as isotropic (red colored), otherwise they are anisotropic (green colored).

The analysis showed that isolated astrocytes from serum-deprived cultures had 40% isotropic regions in their cell bodies, while those from serum-containing cultures exhibited approximately 70% isotropy (Fig. 2 (g)-(h)). Although the exact number of cells in each group could not be determined due to clustering, the number of isolated cells was nearly double in the serum-free culture compared to the other group, suggesting a higher number of isolated cells in the serum-free setting.

V. Discussion

The U-Net model with inception layers in the encoder achieved the highest performance, as shown in Table I. This result was expected, as the multi-scale approach of inception layers enhances the capture of diverse astrocyte characteristics, which improves segmentation accuracy. Segmenting cells in crowded regions presented a challenge due to U-Net's tendency for over-segmentation. Despite testing various architectures about that issue, including Residual and Inception layers, no significant advantage was found among them. However, carefully selecting loss functions improved segmentation of adjacent cells (Fig. 3).

In comparing network architectures for segmentation accuracy, inception layers notably enhanced results, while

Residual layers had minimal impact, mainly reducing over-segmentation. Unet++ faced similar over-segmentation issues. Unet-VGG19 under-performed compared to Unet-VGG16, likely due to over-fitting associated with VGG19's increased complexity. VGG16's slightly shallower architecture demonstrated better resistance to over-fitting.

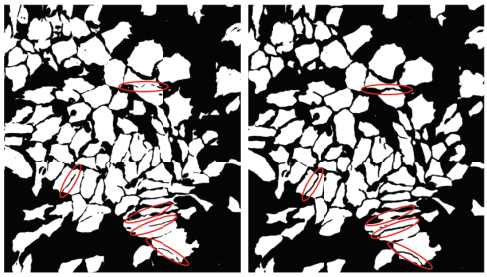

Fig. 3: Segmentation performance improvement on adjacent cells when inception layers are included in encoder of U-Net architecture. (a) Result from the U-Net-VGG16 model, (b) Result from the U-Net-Inceptionv4. The significant improvements are shown with the red ellipses.

Analysis of the experimental dataset highlighted the morphological effects of serum deprivation on astrocytes, consistent with existing literature [19]. Although serum-deprived cells showed higher average anisotropy, isotropic cells were still present, suggesting that serum deprivation causes some cells to become more fibrillous while others maintain isotropy. This variation may indicate different astrocyte subgroups with distinct functionalities.

Our postprocessing step, particularly connected component analysis, proved sensitive to parameter settings. Future work could focus on developing a more stable postprocessing method and automating parameter estimation to enhance robustness. Additionally, while the model was not trained or fine-tuned with the experimental dataset due to limited labeled samples, the performance could improve with more labeled astrocytes from various culture conditions.

We presented a segmentation model for astrocytes in fluorescently labeled microscopy images, achieving an 83% F1 score. The method is supported by directional morphology analysis, revealing the impact of horse serum on astrocyte morphology. By automating segmentation and morphological analysis, our approach reduces manual errors and facilitates processing large datasets, offering a new perspective for neuroscience research.

ACKNOWLEDGEMENT

Authors thanks Esra Nur Yiğit from Medipol REMER for useful discussions and for providing microscopy images. This study was funded by the Scientific and Technological Research Council of Turkey (TUBITAK) ARDEB 3501 Grant No 122E429.

REFERENCES

[1] F. He and Y. E. Sun, "Glial cells more than support cells?" The International Journal of Biochemistry & Cell Biology, vol. 39, no. 4, pp. 661–665, 2007.

[2] J. A. Stogsdill, J. Ramirez, D. Liu, Y. H. Kim, K. T. Baldwin, E. Enustun, and C. Eroglu, "Astrocytic neuroligins control astrocyte morphogenesis and synaptogenesis," Nature, vol. 551, no. 7679, pp. 192-197, 2017.

[3] A. Almad and N. J. Maragakis, "A stocked toolbox for understanding the role of astrocytes in disease," Nature Reviews Neurology, 2018.

[4] S. Healy, J. McMahon, P. Owens, P. Dockery, and U. FitzGerald, "Threshold-based segmentation of fluorescent and chromogenic images of microglia, astrocytes and oligodendrocytes in FIJI," Journal of Neuroscience Methods, vol. 295, pp. 87-103, 2018.

[5] P. M. Kulkarni, E. Barton, M. Savelonas, R. Padmanabhan, Y. Lu, K. Trett, and B. Roysam, "Quantitative 3-D analysis of GFAP labeled astrocytes from fluorescence confocal images," Journal of Neuroscience Methods, vol. 246, pp. 38-51, 2015.

[6] I. Suleymanova, T. Balassa, S. Tripathi, C. Molnar, M. Saarma, Y. Sidorova, and P. Horvath, "A deep convolutional neural network approach for astrocyte detection," Scientific Reports, vol. 8, no. 1, p. 12878, 2018.

[7] J. Blackburn, M. J. Alves, M. T. Aslan, L. Cevik, J. Zhao, C. M. Czeisler, and J. J. Otero, "Astrocyte regional heterogeneity revealed through machine learning-based glial neuroanatomical assays," Journal of Comparative Neurology, vol. 529, no. 10, pp. 2464-2483, 2021.

[8] P. Sethi, G. Virmani, K. Gupta, S. C. R. Thumu, N. Ramanan, and S. Marathe, "Automated morphometric analysis with SMorph software reveals plasticity induced by antidepressant therapy in hippocampal astrocytes," Journal of Cell Science, vol. 134, no. 12, p. jcs258430, 2021.

[9] K. M. Lee, K. B. Chiu, N. A. Renner, H. A. Sansing, P. J. Didier, and A. G. MacLean, "Form follows function: astrocyte morphology and immune dysfunction in SIV neuroAIDS," Journal of Neurovirology, vol. 20, pp. 474-484, 2014.

[10] C. B. Kayasandik, W. Ru, and D. Labate, "A multistep deep learning framework for the automated detection and segmentation of astrocytes in fluorescent images of brain tissue," Scientific Reports, vol. 10, no. 1, pp. 1-12, 2020.

[11] O. Ronneberger, P. Fischer, and T. Brox, "U-net: Convolutional networks for biomedical image segmentation," in International Conference on Medical Image Computing and Computer-Assisted Intervention, Cham: Springer, 2015, pp. 234-241.

[12] K. Simonyan and A. Zisserman, "Very deep convolutional networks for large-scale image recognition," arXiv preprint arXiv:1409.1556, 2014.

[13] Z. Zhou, M. M. Rahman Siddiquee, N. Tajbakhsh, and J. Liang, "Unet++: A nested u-net architecture for medical image segmentation," in Deep Learning in Medical Image Analysis and Multimodal Learning for Clinical Decision Support, Cham: Springer, 2018, pp. 3-11.

[14] C. Szegedy, S. Ioffe, V. Vanhoucke, and A. Alemi, "Inception-v4, inception-resnet and the impact of residual connections on learning," in Proceedings of the AAAI Conference on Artificial Intelligence, vol. 31, no. 1, 2017.

[15] C. H. Sudre, W. Li, T. Vercauteren, S. Ourselin, and M. J. Cardoso, "Generalised dice overlap as a deep learning loss function for highly unbalanced segmentations," in Deep Learning in Medical Image Analysis and Multimodal Learning for Clinical Decision Support, Cham: Springer, 2017, pp. 240-248.

[16] T. Y. Lin, P. Goyal, R. Girshick, K. He, and P. Dollár, "Focal loss for dense object detection," in Proceedings of the IEEE International Conference on Computer Vision, 2017, pp. 2980-2988.

[17] C. B. Kayasandik and D. Labate, "Improved detection of soma location and morphology in fluorescence microscopy images of neurons," Journal of Neuroscience Methods, vol. 274, pp. 61-70, 2016.

[18] D. Labate, P. Negi, B. Ozcan, and M. Papadakis, "Directional ratio based on parabolic molecules and its application to the analysis of tubular structures," in Wavelets and Sparsity XVI, vol. 9597, SPIE, 2015, pp. 159-167.

[19] D. J. Petrović, D. Jagečić, J. Krasić, N. Sinčić, and D. Mitrečić, "Effect of fetal bovine serum or basic fibroblast growth factor on cell survival and the proliferation of neural stem cells: The influence of homocysteine treatment," International Journal of Molecular Sciences, vol. 24, no. 18, p. 14161, 2023.